We are IntechOpen,
the world's leading publisher of
Open Access books
Built by scientists, for scientists

6,900
Open access books available

186,000
International authors and editors

200M
Downloads

154
Countries delivered to

Our authors are among the

TOP 1%
most cited scientists

12.2%
Contributors from top 500 universities

CLARIVATE ANALYTICS
BOOK CITATION INDEX
INDEXED

WEB OF SCIENCE™

Selection of our books indexed in the Book Citation Index
in Web of Science™ Core Collection (BKCI)

Interested in publishing with us?
Contact book.department@intechopen.com

Numbers displayed above are based on latest data collected.
For more information visit www.intechopen.com

Adsorption Cycle and Its Hybrid with Multi-Effect Desalination

Muhammad Wakil Shahzad, Kyaw Thu, Ang Li,
Azhar Bin Ismail and Kim Choon Ng

Additional information is available at the end of the chapter

http://dx.doi.org/10.5772/60400

Abstract

Adsorption (AD) cycle is recently pioneered for cooling and desalination applications. For water treatment, the cycle can be used to treat highly concentrated feed water, ranging from seawater, ground water, and chemically laden waste water. This chapter presents a review of the recent development of AD cycle and its hybridization with known conventional cycles such as the MED and MSF. We begin by looking at the basic sorption theory for different adsorbent–adsorbate pairs, namely the silica gel–water and the zeolite–water pairs. Under the IUPAC categorization, there are six types of isotherm behavior that capture almost all types of adsorbent–adsorbate behaviors and many isotherm correlations have been developed to described their uptake patterns, namely the Henry, Langmuir, Toth, etc. We have recently developed a correlation that can universally capture all six types of isotherms of IUPAC and it requires only four regression coefficients.

We present also the basic AD cycle for seawater desalination as well as its hybridization with known conventional thermally driven cycles. We present the performances of the AD pilot which was powered by renewable solar thermal input. Owing to thermodynamic synergy between the thermally driven cycles, the AD cycle is combined with the robust multi-effect distillation cycle to improve the water production yields. The hybrid cycle is called the "MED+AD" or MEDAD in short. With hybridization, it allows the bottom-brine temperature of the MED to operate below ambient temperature, as low as 5°C, in contrast to the conventional MED which is limited by the ambient, resulting in a quantum increase of distillate production by two to three times. We demonstrate this efficiency improvement in a pilot comprising

a three-stage MED and AD plant and the top-brine temperature is maintained at 70°C. Lastly, we present the concept of exergy to apportion the operating cost of fuel input in a cogeneration plant where both electricity and water are being produced, and this concept gives an operating cost of fuel input to be lower than the conventional enthalpic approach.

Keywords: Thermal Desalination, Adsorption Desalination (AD), Exergy Analysis, Multi-Effect Distillation (MED), Hybrid Cycles

1. Introduction

Fresh water is a precious entity which is needed for economic development of every sector of a country such as agriculture, industrial, and domestic sectors. The persistent quest of economic development and exponential population growth in many countries has intensified the water demand which is projected to grow annually at a rate of 3–4% [1–3]. Even though 70% of the earth is covered by water, most of the part is in nonpotable state due to its salinity, either in the form of brackish, waste, and seawater [3–7]. About 20% of the world population is living below the acute water poverty level of 500 m³ per capita per year [8], risking their health due to poor water quality and substandard sanitation. The demand for fresh water in 2030 is expected to increase up to 6,900 billion cubic meters (Bm³), as compared to total available water resources of 4,500 Bm³ [9]. The fresh water supply and demand scenario is shown in Figure 1, and it is predicted that the sustainable natural water cycle of our earth cannot meet the projected future water demand.
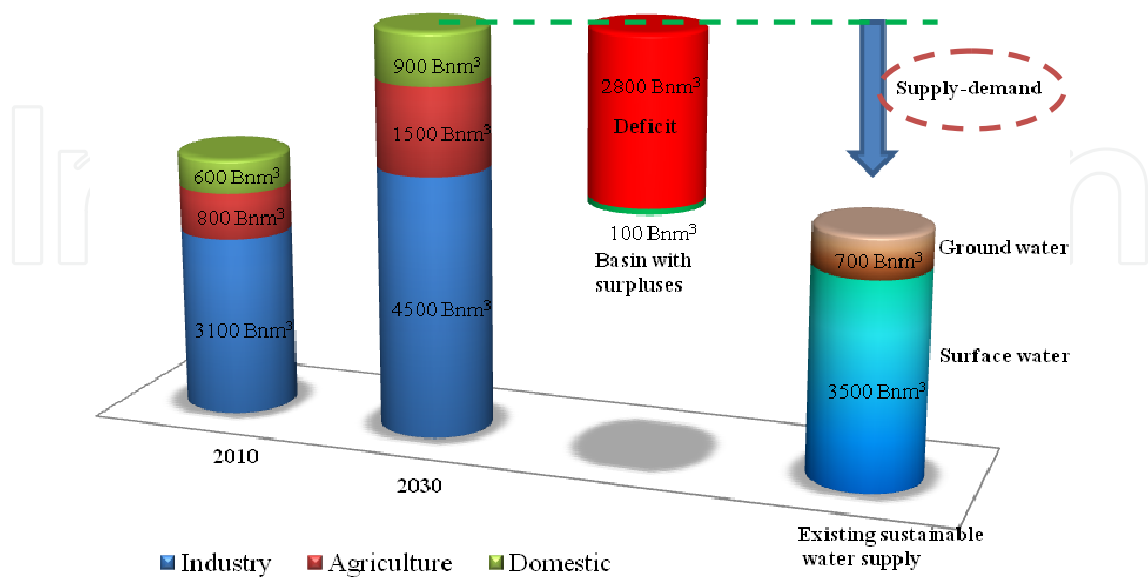

Figure 1. Fresh water supply demand gap: current and future estimates

In 2012, installed desalinated water capacity was 72 Mm^3/day (mcmd) and it is estimated to increase to 98 mcmd by 2015 as reported in the literature [10]. Almost half of total desalination capacity is installed in the Gulf Cooperation Council (GCC) countries. In the 1960s and 1970s, many GCC countries relied heavily on the ground water supply for all sectors such as agriculture, industrial, and domestic sectors. However, the ground water resource in these countries has depleted rapidly over the decades due to excessive water extraction and insufficient aquifer recharge. Despite a higher desalination market share in GCC, the fresh water availability is dropping rapidly to below the acute water poverty level of 500 m^3 per capital per year, caused by an exponential population growth and higher GDP thrust.
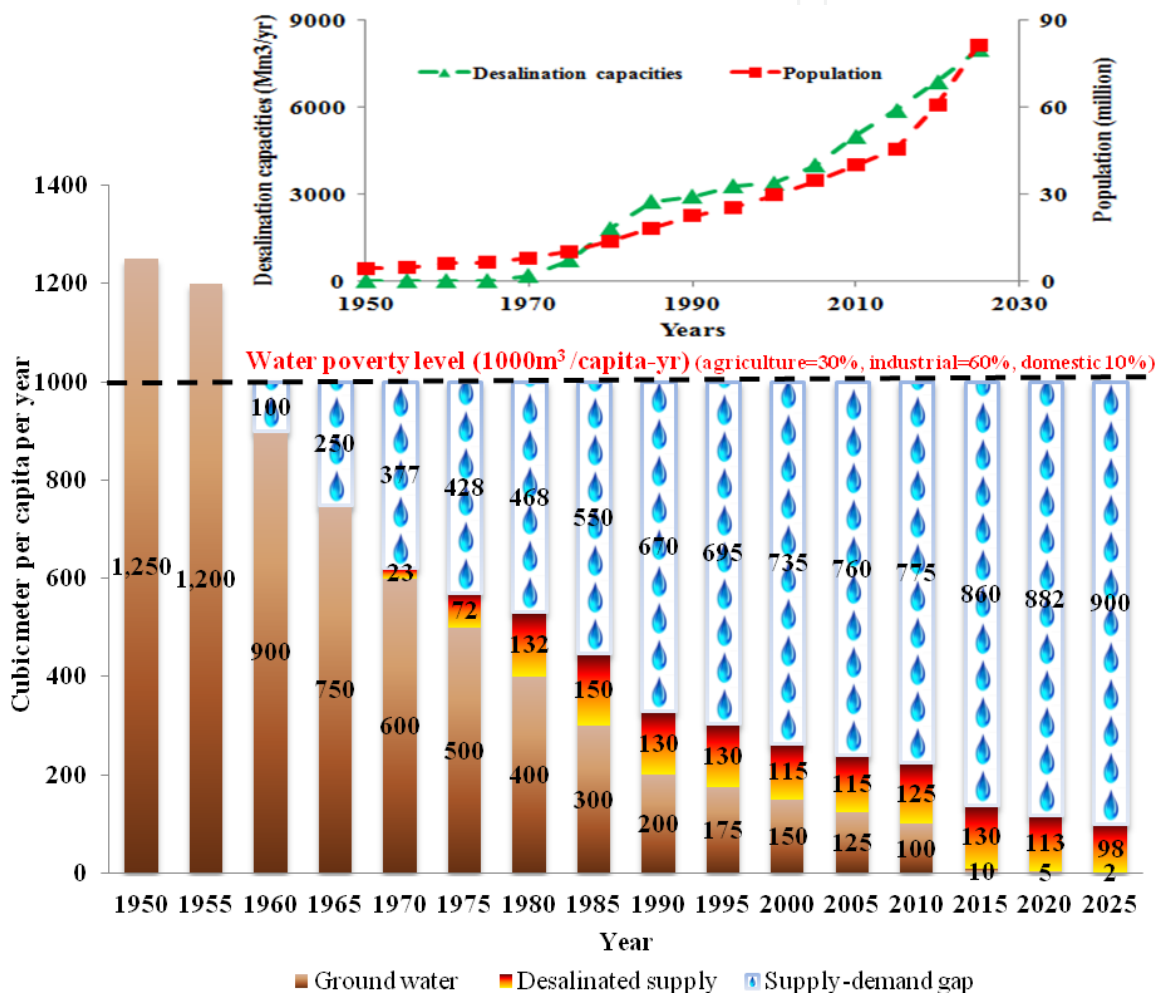

Figure 2. Fresh water availability per capita in GCC countries

GCC countries population, fresh water availability, and desalination scenario are shown in Figure 2, spanning from the early decades in 1950 to the future years up to 2025 [11–17]. Seawater desalination was started in GCC countries in the 1960s, but significantly desalinated water supply was observed in the past two decades, contributing to the overall water consumption share. Increasing trend of desalination capacities has resulted in higher energy consumption, more than 25% of total energy production in GCC countries. It is estimated that,

with contracted desalination facilities, the total primary energy requirement will grow up to 255.45 GWh in 2025 with 55% increment as compared to 112.47 GWh in 2000 and CO_2 emission will be doubled in 2025 as compared to 60 ktonne/year in 2000 as shown in Table 1. The income loss attributed to desalination was 3.6 billion USD in 2000 and this loss is expected to rise to 31 billion USD in 2025 as calculated by considering yearly fuel price in terms of US$/bbl as shown in Table 1.

Year	Specific energy utilization for desalination (GWh_pe)	CO_2 production on the basis of fuel (0.527 tonne/MWh) (ktonne/yr)	Displaced income due to desalination (1 bbl = 1628kWh), (million USD)
1970	6.32	3.3	517.2
1975	25.19	13.3	2066.0
1980	62.29	32.8	5107.6
1985	92.79	48.9	5103.7
1990	98.26	51.8	3930.6
1995	109.92	57.9	2748.0
2000	112.47	59.3	3598.9
2005	131.93	69.5	7256.2
2010	163.96	86.4	13116.6
2015	191.21	100.8	21989.5
2020	221.97	117.0	26636.7
2025	255.45	134.6	31164.5

Table 1. Specific energy consumed and CO_2 footprint in GCC countries due to desalination processes

Water production by desalination processes has significant effect on the energy requirement and environment. The intricate nexus between water, energy, and environment has encouraged scientists and engineers to innovate desalination methods with better energy efficiency and environment-friendly processes. Although RO processes are energy-efficient and dominantly used, they have certain limitations with respect to local conditions. For example, the frequent maintenance issues from high operating pressure; water quality problems in term of residuals of boron, chlorides, and bromides; and severe fluctuations in the seawater intake quality are some of the challenges faced by the RO membranes. In the GCC region, frequent occurrence of harmful algae blooms (HABs) that may contain neuroparalytic and diarrhetic toxins which can pass through the pores of membranes lead to health problems. Large fluctuations in the feed water quality have direct implication to the operation and maintenance costs of RO plants [18–20]. Owing to the uncertainty of RO operation, thermal desalination

methods are deemed as the dominant processes employed in desalination market in the Middle East countries, more than 65% of installed capacities.

An innovative solution to strengthen the thermally driven and yet robust multi-effect desalination (MED) is its integration with the heat-driven adsorption desalination (AD) cycle. AD cycle is an emerging low-cost desalination system that requires only low temperature waste heat or solar energy to operate the cycle. The hybridization of both cycles, called MEDAD, extend the range of downstream (last stage) temperature of conventional MED system typically from 40°C to 5°C. The additional number of stages enhances the water production of the MED cycle by 2 - 3 fold at the same top-brine temperatures. In addition, AD integration cycle has the following advantages: (i) it increases inter-stage temperature differential of each MED stages due to the lowering of the bottom-brine temperature; (ii) it helps to scavenge the ambient energy in last part of the MED stages where the latent energy is further recycled; (iii) the AD cycle utilizes only low temperature waste heat; (iv) it has almost no major moving parts; (v) it reduces the chances of corrosion and fouling due to high concentration exposed to low temperature (5°C) in the last stages; (vi) it produces additional cooling effect from last stages of MED operating below ambient temperature; and (vii) significant increase in system performance. The basics of adsorption phenomenon, AD cycle, and its hybrids and desalination processes economics are presented in detail in this chapter.

2. Basic adsorption phenomena

The understanding of an AD cycle is predicated on the availability of basic equilibria–vapor uptake or isotherms of an adsorbent–adsorbate pair at assorted pressures and temperatures. From literature, all isotherms of adsorbent–adsorbate pairs can be categorized into six types (IUPAC) and they are described by many types of empirical and semi-empirical models. The simplest adsorption isotherm model is the classical Langmuir model [21] where it assumes a homogeneous surface with a monolayer vapor uptake where all adsorbent surfaces contain a uniform charged energy. Each pore vacant site is assumed to be filled by a single vapor molecule, forming a single sorption event. Invoking the rate of gas molecules filling the adsorption sites ($\frac{\mathrm{d}\theta}{\mathrm{d}t}$), as given by Ward and co-workers [22–25], the expression of the Langmuir isotherm model can be derived as follows:

$$
\frac{\mathrm{d}\theta}{\mathrm{d}t} = K' \left[\exp\left(\frac{\mu_g - \mu_\alpha}{RT} \right) - \exp\left(\frac{\mu_\alpha - \mu_g}{RT} \right) \right]
\tag{1}
$$

where μ is the chemical potential in kJ/mol and subscripts g and a are the gaseous and adsorbed phases, T is the absolute temperature, and K' is the dimensionless constant. The isotherm, θ, can be obtained by integrating the rate equation over the energy level from E_c to infinity and in this simple case, when $\rightarrow 0$ then $\theta \rightarrow 0$, and as P is large, θ approaches 1.

$$\theta = \frac{K \exp\left(\dfrac{\varepsilon}{RT}\right) P}{1 + K \exp\left(\dfrac{\varepsilon}{RT}\right) P} \tag{2}$$

A real solid surface of an adsorbent contains geometrical roughness that is formed during its formation or activation process and the energetic heterogeneity has to be accounted for. The gas molecules experienced varying potential at adsorption sites of uneven energy levels and the surfaces are subdivided into infinitesimal pieces. Thus, the total adsorption of a heterogeneous surface is the sum of the product of the sorption event or surface coverage, $\theta(\varepsilon_i)$ and its probability energy distribution, $\chi(\varepsilon_i)$, i.e.,

$$\theta = \sum_i \chi(\varepsilon_i) \cdot \tilde{\theta}(\varepsilon_i) = \int_0^\infty \chi(\varepsilon) \cdot \tilde{\theta}(\varepsilon) d\varepsilon \tag{3}$$

where the Langmuir model can be applied with a probability function over the entire surface being summed to unity, i.e.,

$$\int_0^\infty \chi(\varepsilon) \cdot d\varepsilon = 1 \tag{4}$$

Applying a condensation approximation at moderate temperature, the local surface coverage can be simplified to a step-like dirac-delta function as shown in Figure 3, and expressed below;

$$\lim_{T \to 0} \tilde{\theta}(\varepsilon) = \begin{cases} 0 \text{ for } \varepsilon < \varepsilon_c \\ 1 \text{ for } \varepsilon \geq \varepsilon_c \end{cases} \tag{5}$$

where, ε_c relates to the adsorption energy in equilibrium conditions. Hence, Equation 3 can be simplified to

$$\begin{aligned} \theta &= \int_0^{\varepsilon_c} 0 \cdot \chi(\varepsilon) d\varepsilon + \int_{\varepsilon_c}^\infty 1 \cdot \chi(\varepsilon) d\varepsilon \\ &= \int_{\varepsilon_c}^\infty \chi(\varepsilon) d\varepsilon \end{aligned} \tag{6}$$

A solution of $\chi(\varepsilon)$ to represent the site energy allocation for a real adsorbent surface is obtained by approximating it to a continuous probability distribution function. Depending on the adsorbent surface energy characteristics during adsorption interactions, symmetrical or asymmetrical Gaussian functions are usually assumed, as illustrated in Figure 4.
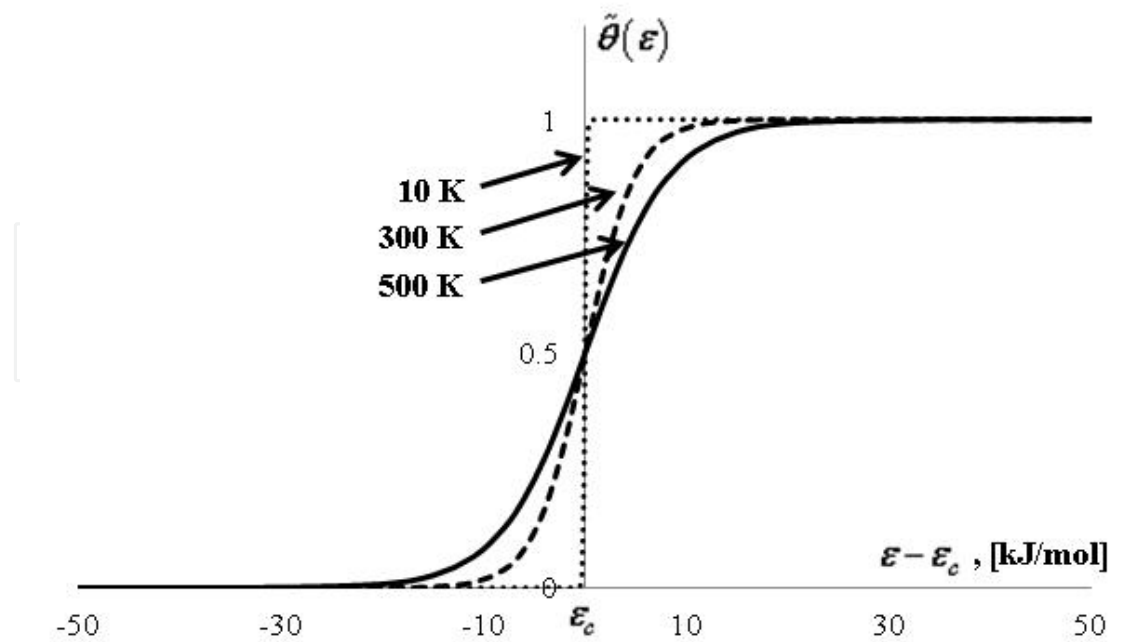
Figure 3. Step-like profile yielded from Equation 5 at moderate temperatures
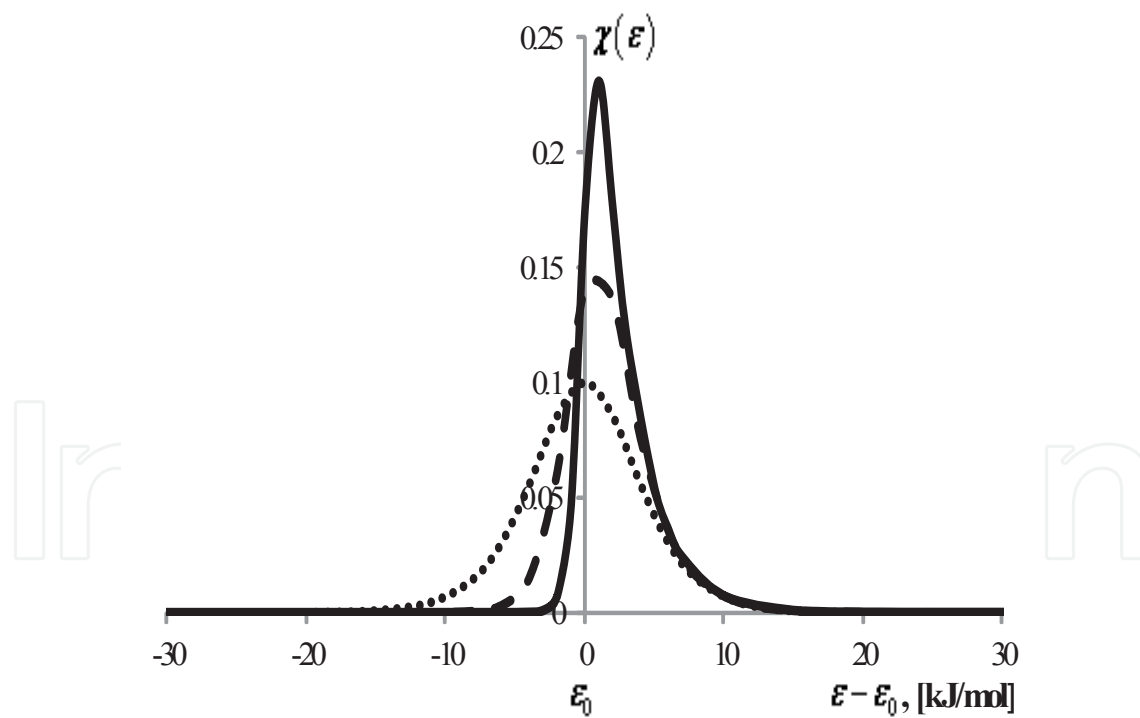
Figure 4. An illustration of symmetrical or asymmetrical Gaussian function to represent the adsorption site energy distribution for classical isotherm models

The details of EDFs, $\chi(\varepsilon)$, for the classic Langmuir–Freundlich [26], Dubinin–Astakhov [27], Dubinin–Raduskevich [28], and Tóth isotherm models are outlined in Table 2, and integrating

EDFs from the cut-off energy ε_c to ∞, the exact correlation of these isotherm models can be obtained.

Model Name	Adsorption Site Energy Distribution $\chi(\varepsilon)$	Isotherm Equation
Langmuir–Freundlich	$\chi(\varepsilon) = \dfrac{\dfrac{1}{c}\exp\left(\dfrac{\varepsilon - \varepsilon_0}{c}\right)}{\left[1 + \exp\left(\dfrac{\varepsilon - \varepsilon_0}{c}\right)\right]^2}$	$\theta = \dfrac{\left[KP\exp\left(\dfrac{\varepsilon_0}{RT}\right)\right]^{\frac{RT}{c}}}{1 + \left[KP\exp\left(\dfrac{\varepsilon_0}{RT}\right)\right]^{\frac{RT}{c}}}$
Dubinin–Astakhov		$\chi(\varepsilon) = \dfrac{r(\varepsilon - \varepsilon_1)^{r-1}}{E^r}\exp\left[-\left(\dfrac{\varepsilon - \varepsilon_1}{E}\right)^r\right]$ $\theta = \exp\left[-\left(\dfrac{RT}{E}\ln\dfrac{P_0}{P}\right)^r\right]$
Dubinin–Radushkevich	$\chi(\varepsilon) = \dfrac{2(\varepsilon - \varepsilon_1)}{E^2}\exp\left[-\left(\dfrac{\varepsilon - \varepsilon_2}{E}\right)^2\right]$	$\theta = \exp\left[-\left(\dfrac{RT}{E}\ln\dfrac{P_0}{P}\right)^2\right]$
Tóth	$\chi(\varepsilon) = \dfrac{\dfrac{1}{RT}\left[\exp\left(\dfrac{\varepsilon - \varepsilon_3}{RT}\right)\right]^t}{\left\{1 + \left[\exp\left(\dfrac{\varepsilon - \varepsilon_3}{RT}\right)\right]^t\right\}^{\frac{t+1}{t}}}$	$\theta = \dfrac{KP\exp\left(\dfrac{\varepsilon_3}{RT}\right)}{\left\{1 + \left[KP\exp\left(\dfrac{\varepsilon_3}{RT}\right)\right]^t\right\}^{\frac{1}{t}}}$

Table 2. Assorted forms of adsorption site energy distribution functions (EDF) for the Langmuir-Freundlich, Dubinin-Astakhov (DA), Dubinin-Raduskevich (DR) and Tóth isotherm models

2.1. Universal site-Energy probability Distribution Function (EDF)

In the recent development of adsorption isotherm theory, Li [29] proposed a universal model that was able to fit all types of isotherms, as specified in Equation 7. Type I to V patterns at various temperatures could be directly captured by the equation with four regression parameters.

$$\frac{q}{q_0} = \frac{A\phi\exp\left(\beta\dfrac{P}{P_s}\right)\dfrac{P}{P_s} + C\dfrac{P}{P_s}}{\left\{1 + \phi\exp\left(\beta\dfrac{P}{P_s}\right)\dfrac{P}{P_s}\right\}^t} \tag{7}$$

and,

$$\beta = \exp\left(\frac{E_c}{RT}\right) \tag{8}$$

$$A = \frac{\left[1 + \phi \exp(\beta)\right]^t - C}{\phi \exp(\beta)} \tag{9}$$

where the alphabet ϕ, C are constants, t is surface heterogeneity factor, and E_c denotes the characteristic energy of the adsorbent–adsorbate pair. These four parameters are required to calculate in the regression process. The rest of the letters have their usual means.

Using the unified adsorption isotherm framework, a universal adsorption site energy distribution function (EDF) was proposed, which relates directly to their isotherm types, and the proposed EDF fitted well with the statistical rate theory of adsorption. The EDF yielded a single peak asymmetrical distribution for Type I which was similar to that for the classical LF, DA, DR, and Tóth isotherm models. The EDF is given as below;

$$\chi(\varepsilon) = \frac{\beta^*}{RT} \left[\phi \exp(\beta^*) \frac{\beta^*}{\beta} + 1\right]^{-t-1} \left\{ \begin{array}{l} \left[A\phi \exp(\beta^*) \dfrac{(\beta^* + 1)}{\beta} + \dfrac{C}{\beta}\right] \\ \left[1 - \phi \exp(\beta^*) \dfrac{\beta^*}{\beta}(t-1)\right] \\ -Ct\phi \exp(\beta^*) \left(\dfrac{\beta^*}{\beta}\right)^2 \end{array} \right\} \tag{10}$$

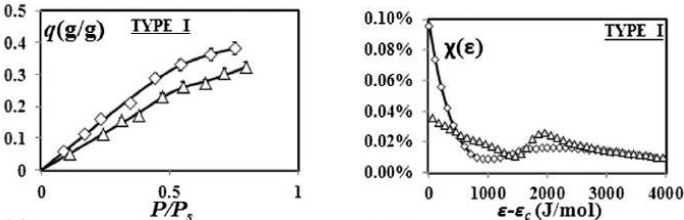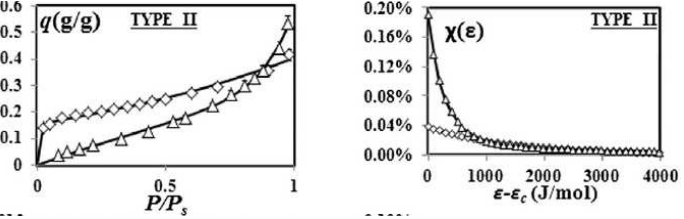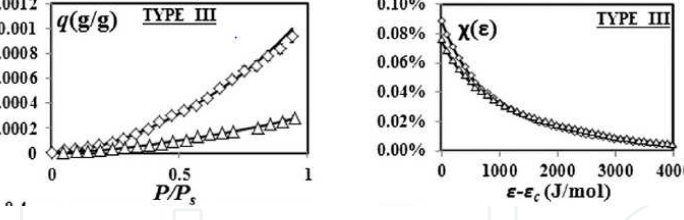where the variable β^* is a function of the adsorption site energy ε and it is expressed as
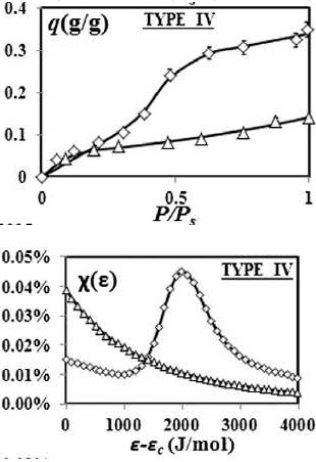
$$\beta^* = \exp\left(\frac{2E_c - \varepsilon}{RT}\right) \tag{11}$$

From the data available from literature and the proposed Eqs. 9 and 10, the assorted isotherms as categorized by the IUPAC can be successfully captured succinctly by these equations using only four coefficients of regression, and these energy distribution functions and isotherms are depicted in Table 3. For each type of isotherm, the corresponding energy distribution functions (EDFs) have been developed.

The adsorbent–adsorbate interaction is the key in the design of adsorption cycle, which can be functionalized to adopt to warmer ambient temperatures, particularly for operation in the summer period of semi-arid or desert regions. Figures 5(a) and (b) depict two major types of useful adsorbents in water uptake: The former is silica gel Type 3A, suitable for an AD cycle operating below 33°C ambient such as tropical weather conditions. The latter figure depicts the isotherms of zeolite (Z0-alumina phosphate oxide, $Al_xPh_YO.nH_2O$). It has properties that can be tailored for adsorption/desorption at ambient temperatures up to 50°C (corresponding to desorption at 3.8–4.5 kPa (60°C isotherm) and adsorption at 2–2.8 kPa (40°C isotherm). The

thermos-physical properties of both adsorbents are tabulated in Table 4, showing the BET surface-pore areas of 600–800 m²/g.

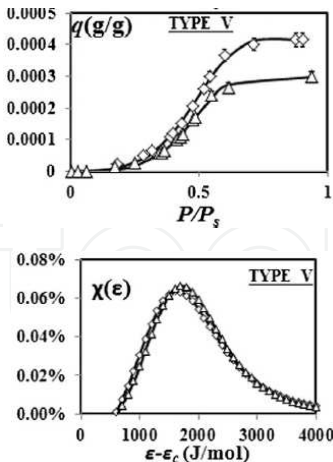| Types of Isotherms (IUPAC Categorization)	Adsorbate–Adsorbent Pair / References
	Type I Water–silica gel Type RD Type I Water–silica gel Type A Qiu J. Characterization of silica gel–water vapor adsorption, MEng Thesis, 2004, NUS
	Type II ◊ Water–boehmite Type II △ Water–polyvinyl pyrrolidone 1. Wang, S-L, Johnston CT, David L, White JL, Stanley LH. Watervapor adsorption and surface area measurement of poorly crystalline boehmite. J Colloid Interface Sci 2003;260(1):26–35. 2. Zhang, J, Zografi G. The relationship between "BET" and "free volume"-derived parameters for water vapor absorption into amorphous solids. J Pharm Sci 2000;89(8):1063–72.
	Type III ◊ Water-sctivated carbon Type III △ Water–carbon S-W nanotube Kim P, Agnihotri S. Application of water-activated carbon isotherm models to water adsorption isotherms of single-walled carbon nanotubes. J Colloid Interface Scie 2008;325(1):64–73.
	Type IV ◊ Water–boehmite Type IV △ Water–polyvinyl pyrrolidone Bansal RC, Dhami TL. Surface characteristics and surface behaviour of polymer carbons—II: adsorption of water vapor. Carbon 1978;16(5):389–95.

Types of Isotherms (IUPAC Categorization)	Adsorbate–Adsorbent Pair / References
	Type II ◇ Water–boehmite Type II △ Water–polyvinyl pyrrolidone Lagorsse S, Campo MC, Magalhaes FD, Mendes A. Water adsorption on carbon molecular sieve membranes: experimental data and isotherm model. Carbon 2005;43(13):2769–79.

Table 3. A summary of the energy distribution functions and isotherms as categorized by the IUPAC
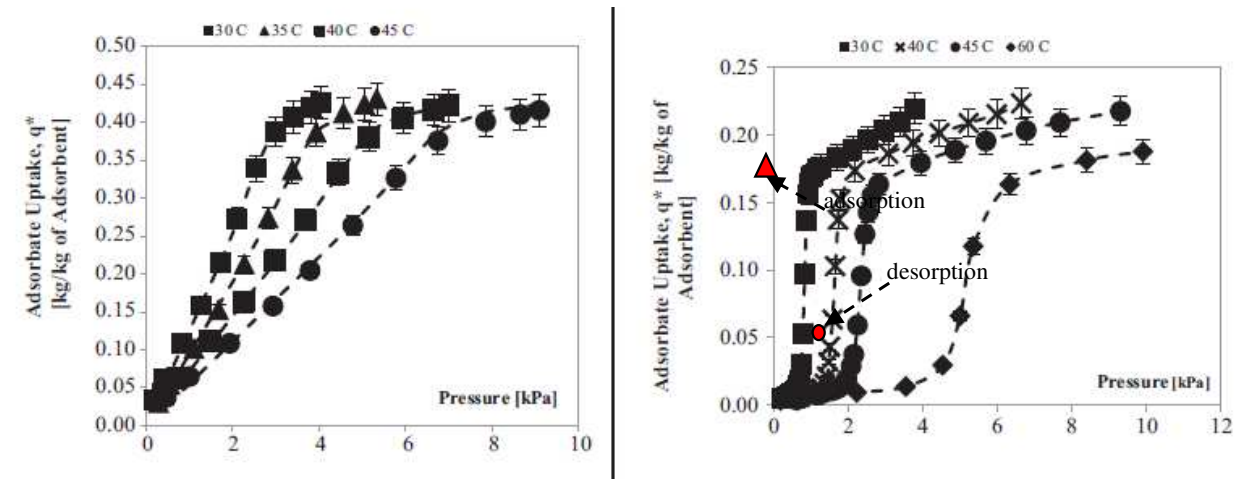

Figure 5. (a) shows the isotherms of water-silica gel Type 3A at four temperatures: 30ºC to 45º C at increasing pressure up to 10 kPa, (b) depicts the isotherms of Zeolite (Z01- Alumina Phosphate Oxide) from 30º C to 60º C.

Properties	Silica Gel Type 3A	Zeolite FAM Z01
BET surface area [m^2/g]	680	147.3
Porous volume [ml/g]	0.47	0.071
Apparent density [kg/m^3]	770	600–700
Thermal conductivity [W/m.K]	0.174	0.113 (30ºC)
Heat of adsorption (H_2O) [kJ/kg of H_2O]	2800	3110 (25ºC)
Specific heat capacity [kJ/kg.K]	0.921	(30ºC)

**Table 4.** Thermo-physical properties of the silica gel type 3A and Zeolite (Z01)

3. Design of AD batch-operated cycle

There are five main components of AD system namely: (i) evaporator, (ii) adsorption and desorption reactor beds, (iii) condenser, (iv) pumps, and (v) pretreatment facility. The detailed process diagram is shown in Figure 6. For the batch-operated AD cycle, it involves two main processes.

3.1. Adsorption-assisted-evaporation

In which the vapors generated in AD evaporator are adsorbed on the pore surface area of adsorbent. The heat source is circulated through the tubes of evaporator and seawater is sprayed on the tube bundle. It is observed that the evaporation is initiated by heat source, but during adsorption process the high affinity of water vapor of adsorbent drops the evaporator pressure and contribute in evaporation. The AD evaporator operation temperature can be controlled by heat source temperature that is normally circulated in terms of chilled water. The AD evaporator can operate at a wide range of chilled water temperature varying from 5°C to 30°C to produce the cooling effect as well at low temperature operation. The vapor adsorption process continues until the adsorbent bed reaches a saturation state.
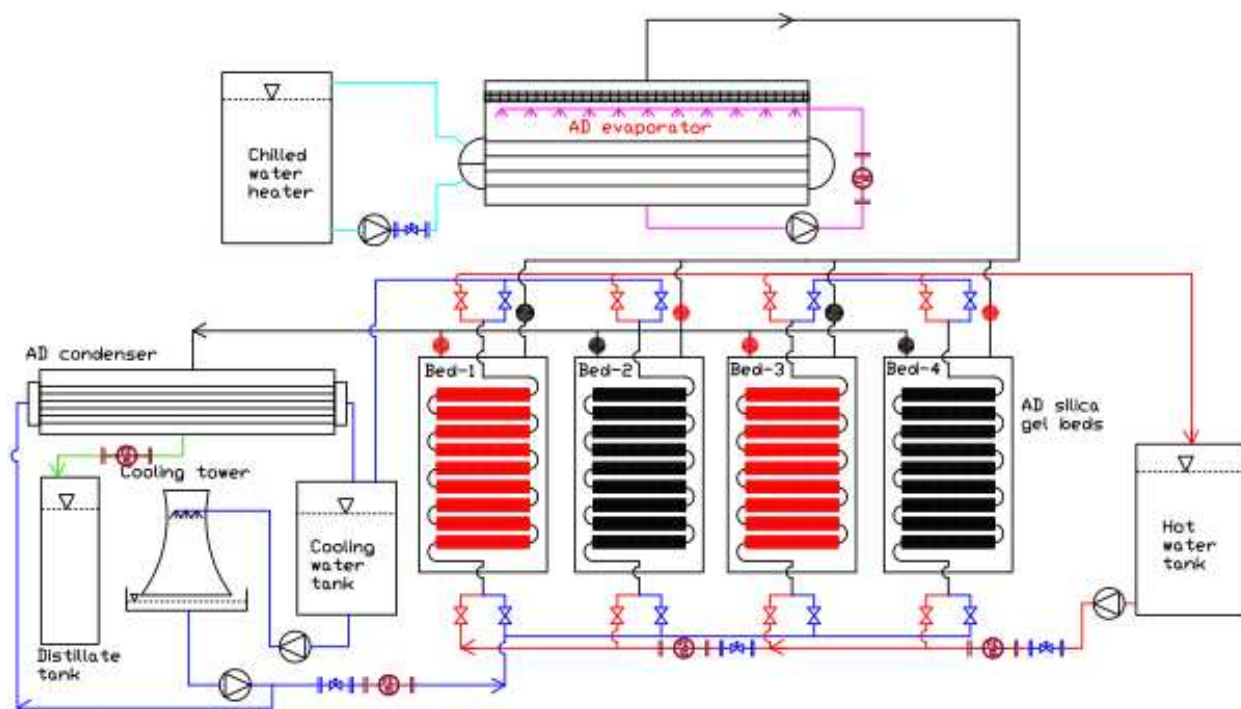
Figure 6. Detailed schematics of an adsorption desalination cycle. The circle (filled) dots are the vapor valves and the pair of triangles refers to the liquid valves. The range of vapor pressures in evaporator and condenser are 1-2 kPa and 5 to 7 kPa

3.2. Desorption-activated-condensation

In which saturated adsorbent is regenerated using the low-grade industrial waste heat or renewable energy (desorption temperature varies from 55°C to 85°C) and desorbed vapors are condensed in a water-cooled condenser and collected as a distillate water.

It can be seen that two useful effects produced by AD cycle are the cooling effect by the first process "adsorption-assisted-evaporation" and fresh water production by converting the seawater by second process "desorption-activated-condensation". Useful effects which are cooling and water production can be produced simultaneously by introducing the multi-bed technique.

In multi-bed AD system, the operation and switching technique is used. During operation, one or pair of adsorbent reactor beds undergo the adsorption process and at the same time one or pair of adsorbent reactor beds execute the desorption process. The time for adsorbent reactor beds operation, either adsorption or desorption, depends on the heat source temperature and silica gel quantity packed in a bed. Prior to changing the reactor duties, there is a short time interval called switching in which the adsorber bed is preheated whilst the desorber bed is precooled to enhance the performance of cycle. In AD cycles, the operation (adsorption and desorption) and switching processes are controlled by automated control scheme that can open and close the respective bed hot/cold water valves. During switching operation, all vapor valves are closed so that there is no adsorption or desorption taking place.

4. MED-AD hybrid cycle

MEDAD is a hybrid of two thermal systems namely multi-effect desalination system and adsorption cycle. The main components of this novel thermal hybrid system are (1) multi-effect distillation (MED) system, (2) adsorption desalination (AD) cycle, and (3) auxiliary equipments. In this hybridization system, the last stage of the MED is connected to adsorption beds of AD cycle for the direct vapor communication to adsorption beds. Figure 7 shows detailed flow schematic of MED plant combined with AD system.

Adsorption-based desalination is investigated by many researchers [30–45] and reported that optimal specific daily water production (SDWP) for four bed scheme is about 4.7 kg/kg silica gel. The first adsorption desalination plant was installed in the National University of Singapore (NUS) which consists of four silica gel beds. Ng et al. investigated the processes using chilled water at assorted temperature and demonstrated that the specific water production of the system [46, 47]. They also introduced and patented a novel hybrid desalination method "MEDAD cycle" that is a combination of conventional MED and AD cycle [48, 49]. This novel desalination cycle can mitigate the limitations of conventional MED system to increase the system performance. This combination allows the MED last stage to operate below ambient temperature typically at 5°C as compared to traditional MED at 40°C. This not only reduces the corrosion chances but also increases the distillate production to almost 2 – 3 fold as compared to traditional MED systems.
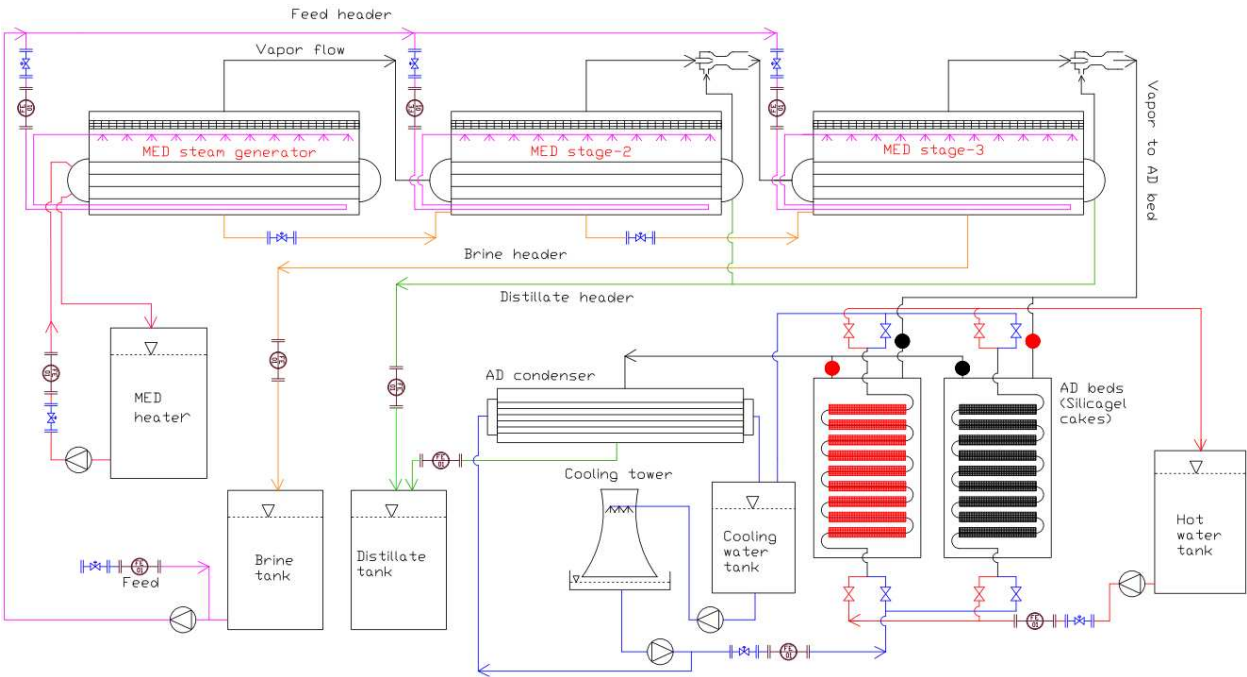
Figure 7. Detailed P& ID diagram for an experimental MED facility of nominal heating capacity of 12 kW. The first stage comprises a water-fired steam generator whilst the last stage (3rd stage) is open to a water-cooled cooling tower

4.1. MED-AD simulation

MEDAD cycle simulation have been conducted [50–53] and presented in Table 5. The simulation is based on a fully transient model and the predicted results are compared with conventional MED system. It is observed that at same input parameters such as a top-brine-temperature (TBT), water production can achieve up to two fold increase when the hybridized MEDAD is compared with the MED cycle alone.

Equation	Remarks
Modeling equations for steam generator	
$$[(M_{hw}.Cp_{hw})]\frac{dT_{hw}}{dt} = \left(\dot{m}_{hw}h_{f,Thw,in}\right) - \left(\dot{m}_{hw}h_{f,Thw,out}\right) - h_{in,o}.A_{in,i}(T_{hw} - T_{tube,i})$$	Energy balance for the hot water flowing inside the tubes of brine heater.
$$[(M_{HX,i}.Cp_{hx,i})]\frac{dT_{tube,i}}{dt} = h_{in,i}.A_{in,i}(T_{hw,i} - T_{tube,i}) - h_{out,i}.A_{out,i}(T_{tube,i} - T_{v,i})$$	Energy balance for metal tubes.
$$\frac{dM_{b,i}}{dt} = \dot{m}_{f,i} - \dot{m}_{b,i} - \dot{m}_{v,i}$$	Mass balance for the seawater inventory in the

Equation	Remarks
	evaporator side of the brine heater.
$Q_{in} = h_{o,i} A_i (T_t - T_{v,i}) [(M_{b,i} . Cp_{b,Tb}) + (M_{HX,i} . Cp_{HX})] \dfrac{dT_i}{dt} = (\dot{m}_{f,i} h_{f,Tf}) - (\dot{m}_{b,i} h_{f,Tb}) - (\dot{m}_{v,i} h_{g,Tv}) + Q_{in,i}$	Energy balance for the evaporator side of the steam generator.
$M_{b,i} \dfrac{dX_{b,i}}{dt} = (\dot{m}_{f,i} X_{f,i}) + (\dot{m}_{b,i} X_{b,i}) - (\dot{m}_{v,i} X_{v,i})$	Material/ concentration balance
$Nu = \dfrac{h_{in,i} d_{in,i}}{K_{tube,i}} = 0.023 Re_l^{0.80} Pr_l^{0.40}$	Convective heat transfer coefficient equation
$R_{wall,i} = \dfrac{\ln\left(\dfrac{d_{out,i}}{d_{in,i}}\right)}{2.\pi.K_{tube,i}.L_{tube,i}}$	Tube wall resistance
$h_o \left(\dfrac{v^2}{k^3 g}\right)^{1/3} = 0.0007\, Re^{0.2}\, Pr^{0.65}\, q''^{0.4}$	Falling film evaporation heat transfer coefficient, Han and Fletcher's correlation
$U_i A_i = \dfrac{1}{\dfrac{1}{h_{in,i} A_{in,i}} + R_{wall,i} + \dfrac{1}{h_{out,i} A_{out,i}}}$	Overall heat transfer coefficient
Modeling equations for intermediate stages	
$[(M_{l,i+1} . Cp_{l,Tcond})] \dfrac{dT_{cond,i+1}}{dt} = [\dot{m}_v h_{fg,Tv}]_i - [h_{in} . A_{in} (T_{cond} - T_{tube})]_{i+1}$	Energy balance for the condenser side of the ith effect
$[(M_{HX,i+1} . Cp_{hx,i+1})] \dfrac{dT_{tube,i+1}}{dt} = h_{in,i+1} . A_{in,i+1} (T_{cond,i+1} - T_{tube,i+1}) - h_{out,i+1} . A_{out,i+1} (T_{tube,i+1} - T_{v,i+1})$	Energy balance for tube metal
$\dfrac{dM_{b,i+1}}{dt} = \dot{m}_{f,i+1} - \dot{m}_{b,i+1} - \dot{m}_{v,i+1}$	Brine inventory balance
$Q_{in,i+1} = h_{out,i+1} A_{i+1} (T_{t,i+1} - T_{v,i+1}) [(M_{b,i+1} . Cp_b) + (M_{HX,i+1} . Cp_{HX,i+1})] \dfrac{dT_{i+1}}{dt} = (\dot{m}_{f,i+1} h_{f,Tf}) - (\dot{m}_{b,i+1} h_{f,Tb}) - (\dot{m}_{v,i+1} h_{g,Tv}) + Q_{in,i+1}$	Energy balance for evaporator side
$M_{b,i+1} \dfrac{dX_{b,i+1}}{dt} = (\dot{m}_{f,i+1} X_{f,i+1}) - (\dot{m}_{b,i+1} X_{b,i+1}) - (\dot{m}_{v,i+1} X_{v,i+1})$	Material/ concentration balance

Equation	Remarks
$$Nu = \frac{h_{in,i+1}L_{i+1}}{K_{tube,i+1}} = 0.728\left[\frac{gh_{fg,Tcond}\rho_{l,Tcond}(\rho_l-\rho_v)_{Tcond}K^3_{l,Tcond}}{\mu_{l,Tcond}d_i(T_{v,i+1}-T_{tube,i+1})}\right]^{1/4}$$	Nusselt film condensation correlation for the calculation of the heat transfer coefficient inside the condenser tubes
$$U_iA_i = \cfrac{1}{\cfrac{1}{h_{in,i}A_{in,i}} + R_{wall,i} + \cfrac{1}{h_{out,i}A_{out,i}}}$$	Overall heat transfer coefficient equation
MED last stage connected with AD beds	
$$[(M_{b,n}.Cp_b) + (M_{HX,n}.Cp_{HX,n})]\frac{dT_n}{dt} = \left(\overset{\bullet}{m}_{f,n}h_{f,Tf}\right) - \left(\overset{\bullet}{m}_{b,n}h_{f,Tb}\right) - (M_{sg}h_{g,Tv})\frac{dq_{ads}}{dt} + Q_{in,n}$$ $$Q_{in,n} = h_{out,n}A_n(T_{t,n}-T_{v,n})$$	Energy balance for the condenser side of the i th effect

Table 5. MEDAD modeling equations

Figure 8 shows the transient temperature profiles of a MEDAD cycle. It can be seen that last stages of MED are operating below ambient temperature due to hybridization. It can also be noticed that MED last stages profiles are affected by cyclic AD operation.
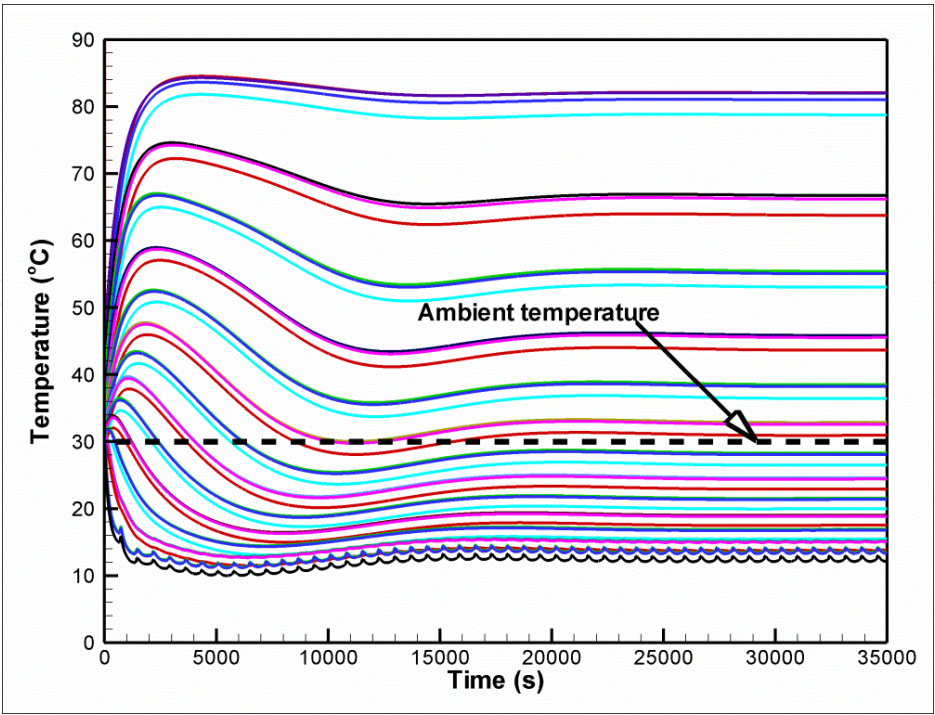

Figure 8. MEDAD cycle components temporal temperature profiles

Figure 9 mapped the performance parameters of hybrid MEDAD cycle (concentration, GOR, PR, and WPR). It can be observed that the batched-mode water vapor uptake by the coupled AD cycle dominates the performance of the cycle. The performance of the MEDAD cycle with different additional effects with the conventional eight effect MED cycle as baseline cycle is studied in terms of water production rate.
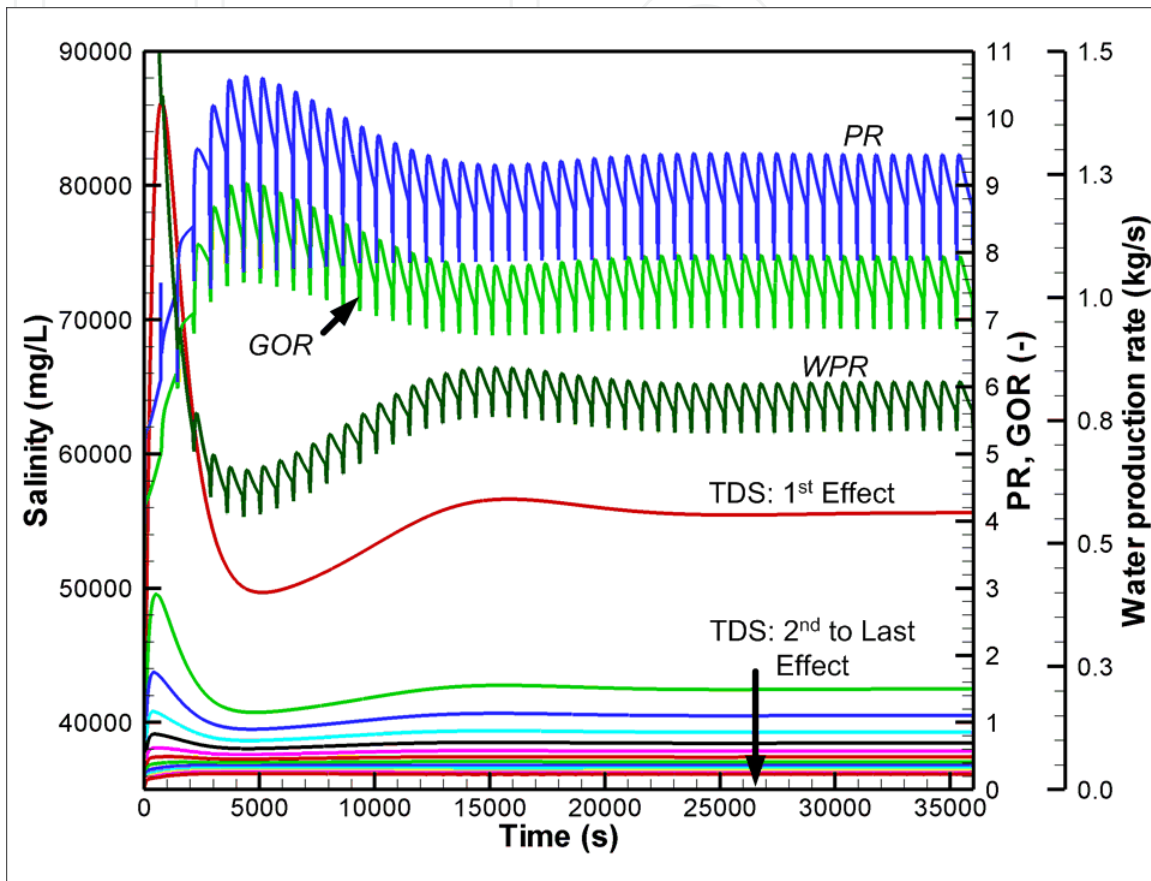
Figure 9. MEDAD hybrid cycle performance (concentration, GOR, PR and WPR)

Figure 10 shows the quantum jump in the water production rate of the proposed MEDAD cycle. Another aspect of this hybridization is that the desorbed water vapor from the AD cycle can be recycled back into the MED system for further energy recovery.

4.2. MED-AD experimentation

A three-stage MED system is designed [54], fabricated, and installed in NUS as shown in Figure 11. In MED stages, vapor emanation from feed seawater is achieved by falling film-evaporation process. Evaporation energy is recovered by series of reutilization of vapor condensing energy in successive stages of those produced in preceding stages. Process of vapor production and energy recovery by condensation continues until the last stage of MED. The vapors from the last stage are then directed toward AD beds where they are adsorbed on the adsorbent surface. Adsorbent high affinity for water vapor drops the pressure and hence the saturation temper-
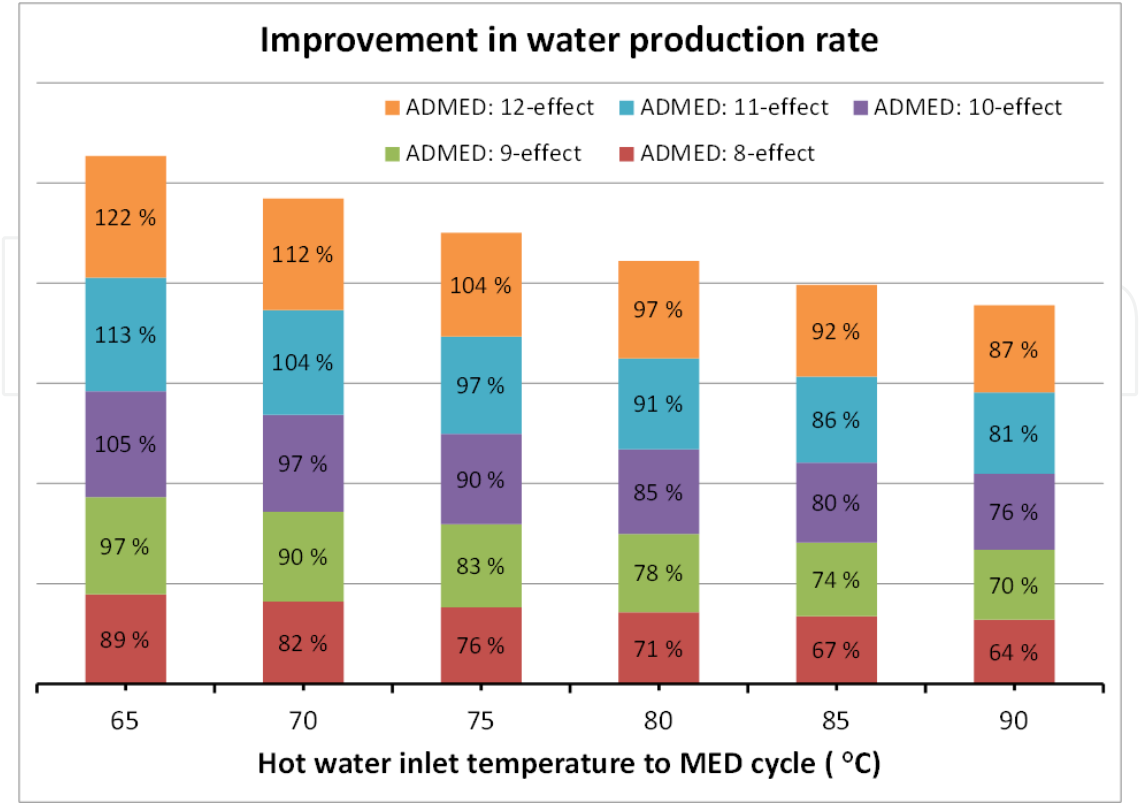
Figure 10. Percentage improvement in water production rate by the MEDAD cycle

ature of last stages falls below ambient, typically up to 5°C. It is observed that this drop in pressure and temperature of last stage also affected the operational parameters of the few preceding stages.

Figure 11. MEDAD system installed in NUS

Experiments are conducted in two steps. In first part, system is operated as a conventional MED at assorted heat source temperature ranges from 38°C to 70°C. In second part, experiments are conducted as a hybrid MEDAD system at assorted heat source temperature ranges from 15°C to 70°C and results are compared with conventional MED system.
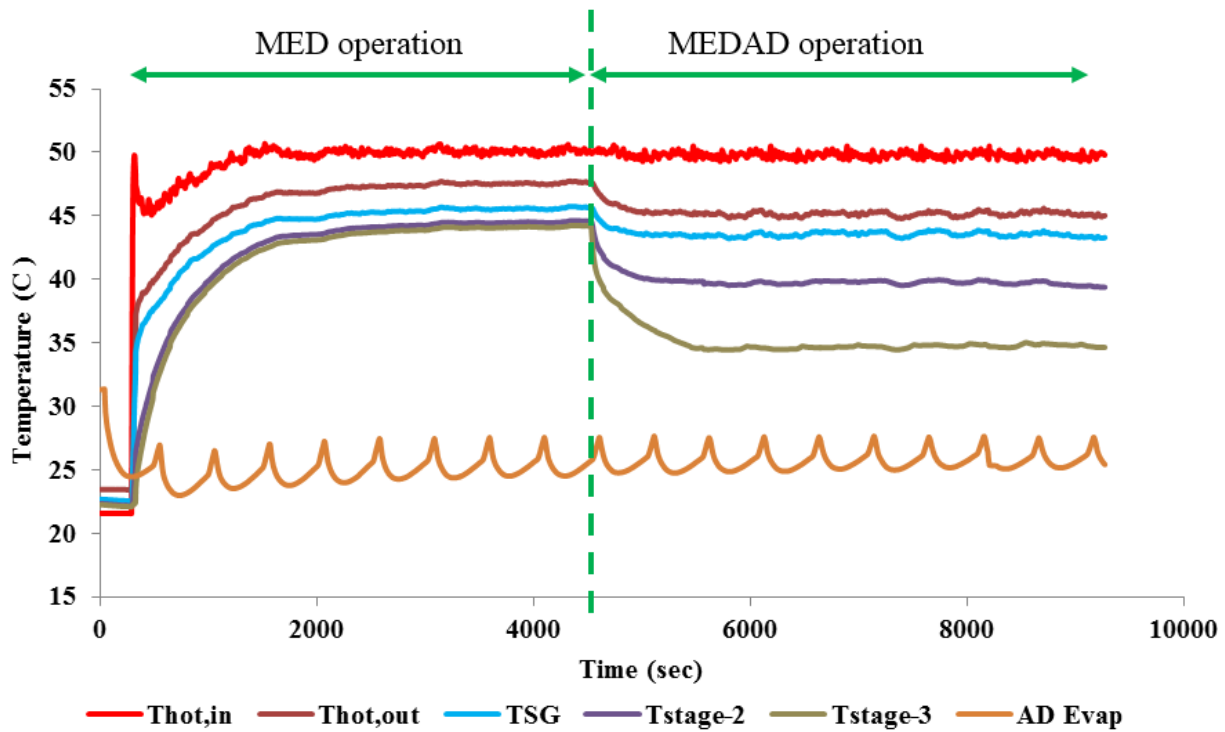

**Figure 12.** MEDAD components temperature profiles at 38°C heat source temperature

Figure 12 shows the instantaneous temperatures of MED and MEDAD components at a heat source temperature of 38°C. It can be seen that steady-state events (minimum temperature fluctuations) occur after 1 hour from start-up and experiments for distillate collection are continued for 4 to 5 hours. It is noticed that the inter-stage temperature difference (ΔT) is more than twice per stage as compared to the conventional MED stages. This is attributed to the vapor uptake by the adsorbent of AD cycle, resulting in the increase of vapor production. The MEDAD cycle yields a stage ΔT from 3°C to 4°C as compared to 1°C or less in the case of MED alone. Table 6 shows the comparison of MEDAD and MED components steady-state temperature values.

Figure 13 shows the distillate production trace at heat source 38°C from MED stages, AD condenser and combined. The batch operated AD production can be seen clearly. At the start of desorption, the production is higher and it drops with time to zero during the switching period while MED stages production is quite stable. Small fluctuations in MED water production may be due to the fluctuations in the spray of the feed that affect the condensation rate. It can be seen that hybridization boost water production 2 – 3 fold as compared to conventional MED system at same TBT. Water production profiles are similar as explained in simulated results.
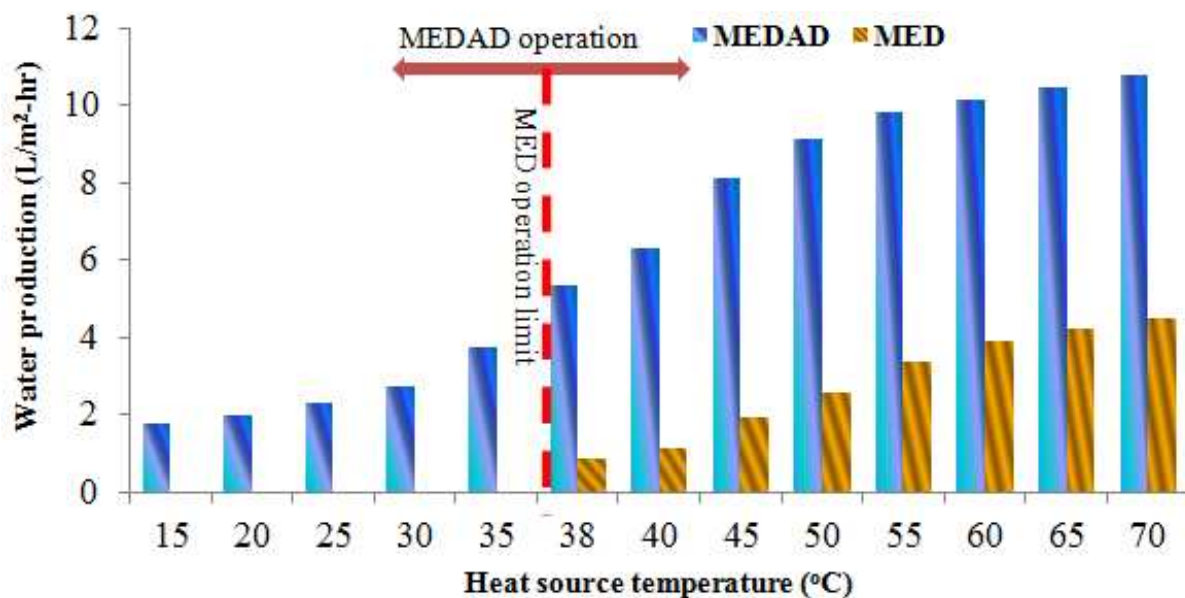
Heat source temperature (°C)	MED	MEDAD	MED	MEDAD	MED	MEDAD	MED condenser	AD evaporator
	SG	SG	Stage-2	Stage-2	Stage-3	Stage-3		
70	63.9	54.4	62.8	50.8	62.3	46.7	56.6	26.1
65	59.6	50.7	58.7	47.0	58.1	42.5	53.9	25.8
60	55.4	49.2	54.4	45.7	53.8	41.3	49.4	25.5
55	51.5	48.5	50.5	44.8	49.9	40.8	45.8	25.1
50	47.4	44.6	46.7	41.6	46.2	37.9	42.7	23.2
45	43.9	41.1	43.4	38.6	43.0	34.9	40.3	22.4
40	38.7	36.6	38.4	34.8	38.1	31.6	36.1	21.0
38	37.4	35.4	37.2	33.5	37.0	30.3	35.3	18.2
Operating limit of Conventional MED. The lower operational points are from MEDAD Hybrids								
35	-	30.9	-	27.9	-	23.5	-	16.1
30	-	26.0	-	23.7	-	19.1	-	12.2
25	-	22.1	-	19.9	-	16.3	-	10.1
20	-	18.1	-	14.2	-	11.3	-	7.1
15	-	13.2	-	11.5	-	9.4	-	5.6

Table 6. A comparison of conventional MED and hybrid MEDAD systems components temperatures at different heat source temperatures
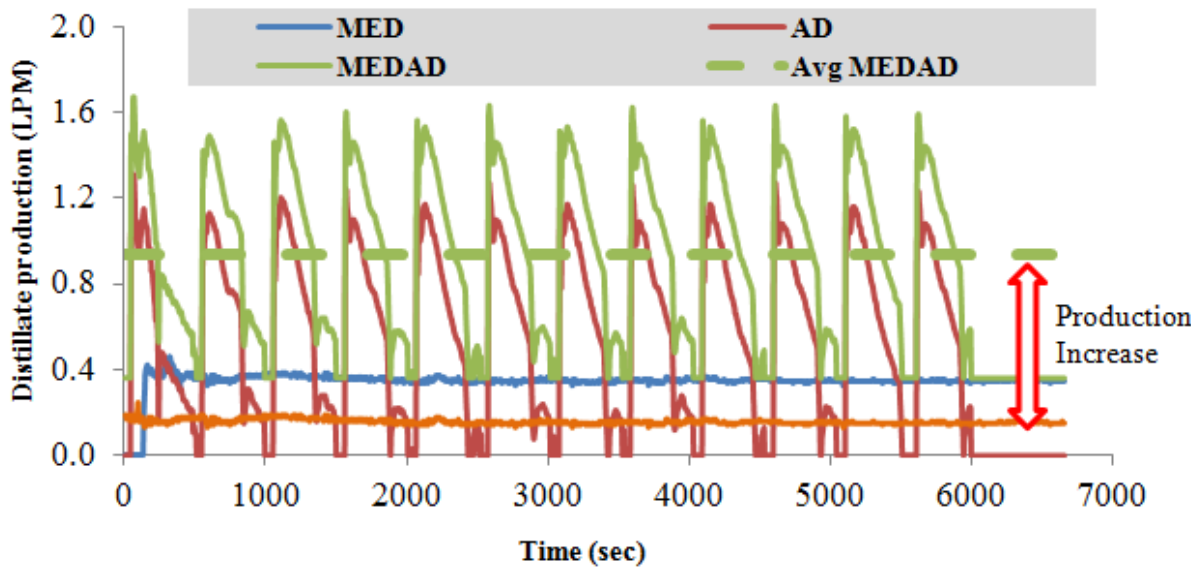
Figure 13. Conventional MED and hybrid MEDAD cycle water production profiles at 38°C heat source temperature

Figure 14. MED and MEDAD steady state water production at different heat source temperatures

Figure 14 shows the comparison of water production of MED and hybrid MEDAD cycles at assorted heat source temperatures. Quantum increase in water production (two- to threefold) can be observed at all heat source temperatures. These results have good agreement with simulation results. It can also be seen that in conventional MED system last stage temperature is limited to 38°C due to condenser operating with cooling water from cooling tower. While in the case of hybrid MEDAD, the last stage temperature can be as low as 5°C because there is no condenser and last stage is connected to AD beds for vapor adsorption. This higher overall operational gap in proposed hybrid MEDAD cycle helps to insert more number of stages (up to 19 stages) as compared to conventional MED system (about 4–6 stages). More number of stages increases the vapor condensation heat recoveries and hence the water production at same top brine temperatures.

5. Exergy analysis for operational cost apportionment

A computation model is developed for the cogeneration plant where the properties of expanding steam, such as enthalpy (h) and entropy (s) at a given temperature and pressure, are computed for the key states in the schematic diagrams of "PP", "PP+MED," and "PP +MEDAD" cycles. The approach employed here is to calculate the total exergy changes or destruction across the inlet and exit sections of the equipment. For example, the exergy associated with the turbines is the sum of all contributions from (a) the HP-T unit at the same mass flow rate across it, (b) the LP-T unit until the extraction point, and (c) the exergy changes after the point of steam extraction, i.e., $E_{T,1-2} = E_{1-a} + E_{b-1'} + E_{1'-2}$. On the basis of total exergy available across whole system, proportion utilized by power plant and desalination system is calculated.

For this comparison study, an assorted range of bled-steam is extracted at low pressure but the mass flow rates are varied to cover the expected practical operational ranges, typically from 10% to 50% of the total flow. At 20% bled-steam from the LP-T, the ratios of power-to-water for exergy and energetic analyses are found to be 95.7%:4.3% (exergy) and 72.2%:27.8% (energetic) methods, respectively. This implies that if the 20% steam were to be continuously consumed by the low pressure turbines (LP-T), its work contribution from LP_T would be insignificant, i.e., a maximum of 4.3%. However, the energetic value of bled-steam accounts for a disproportionate share of 27.8% due primarily to the high latent heat content of the low pressure steam. This ratio of energy-to-exergy shares of the total working steam is found to be 4 – 7 fold higher, descending with the larger amount of bled-steam as shown in Figure 15. The higher effectiveness of working steam incurred at the MED cycle is attributed to the better thermodynamic matching of steam's latent energy.
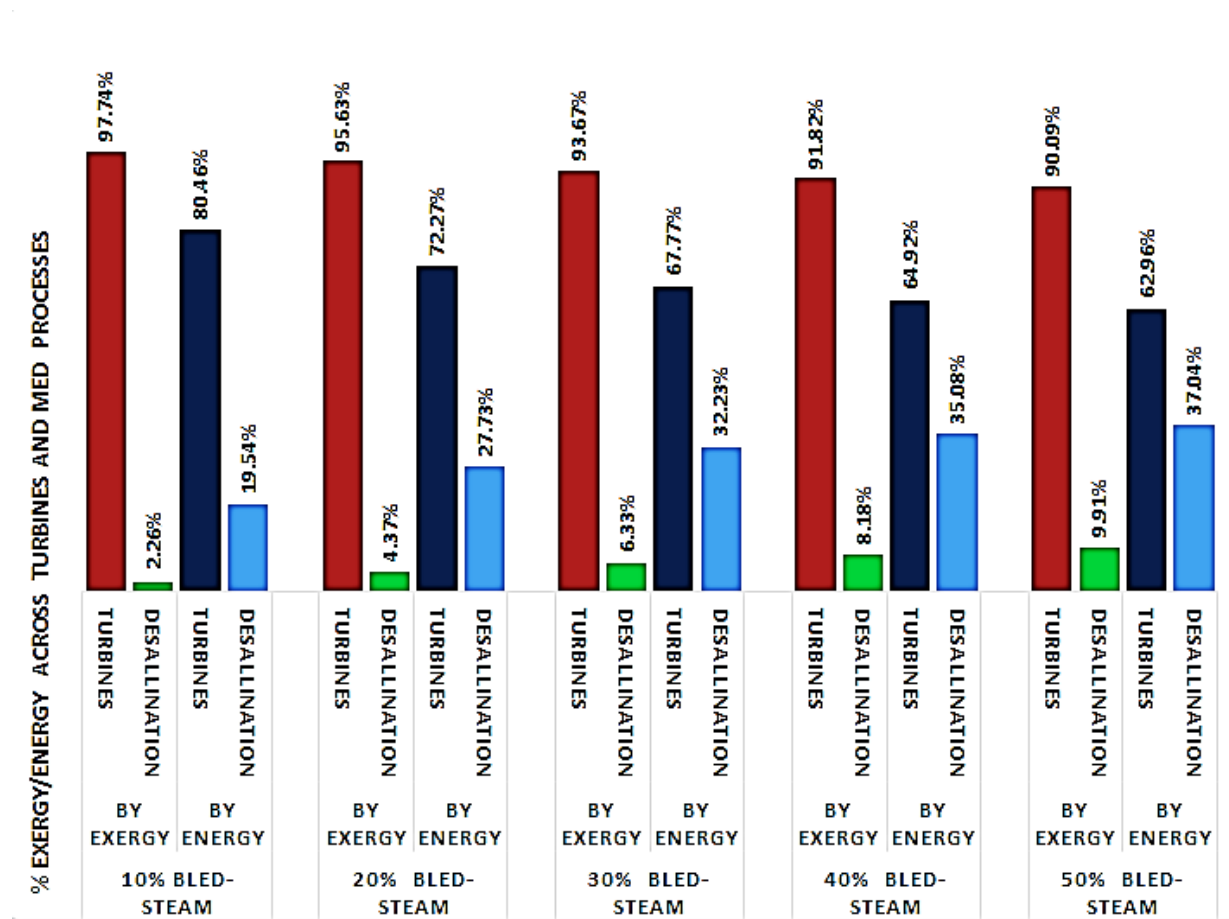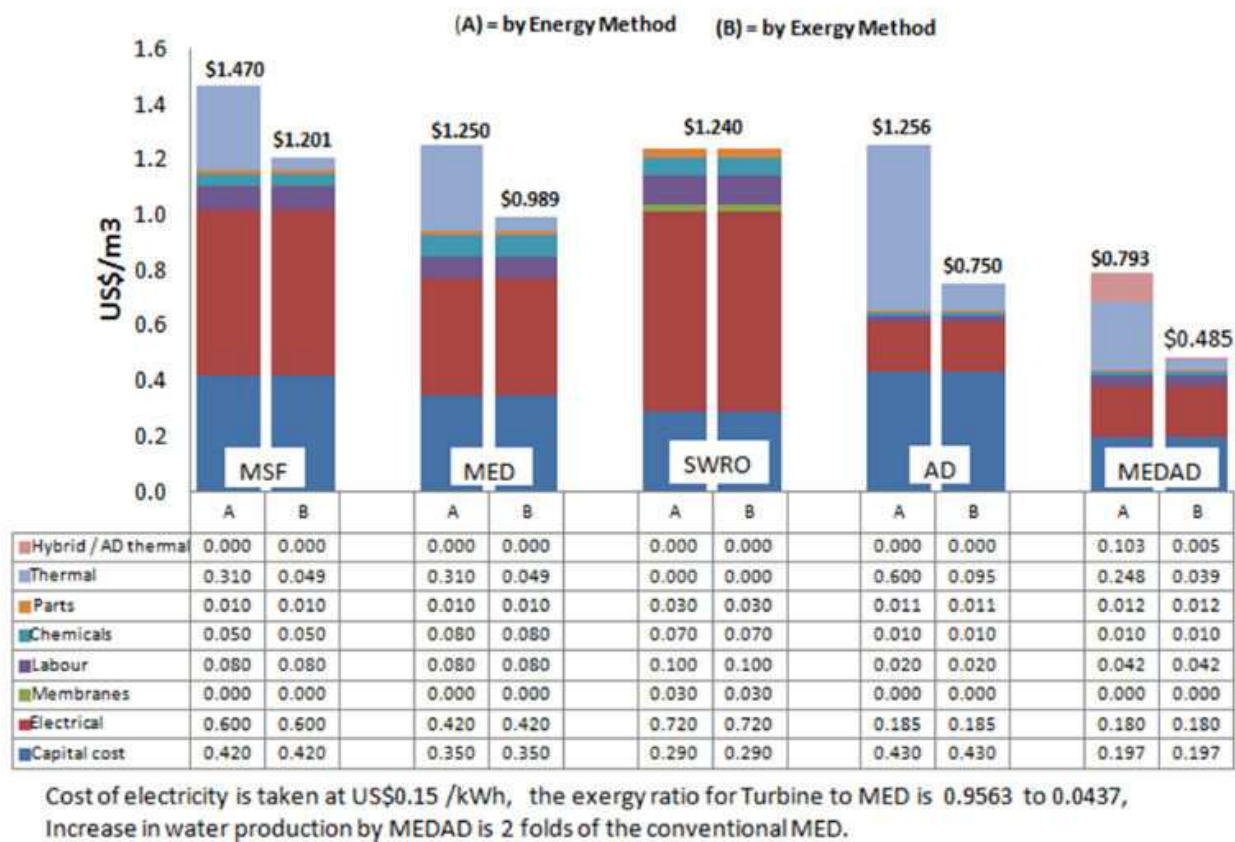

Figure 15. Exergetic and energetic proportions at different percent of steam extraction

On the basis of the above analysis for primary fuel cost and with data from the published literature [55, 56], the life-cycle cost (LCC) of water production is compared for all capital expenditure (Capex) and operation expenditure (Opex), across all proven industrial processes,

	A = by Energy Method	B		A	B		A	B		A	B		A	B
	MSF			MED			SWRO			AD			MEDAD	
Hybrid / AD thermal	0.000	0.000		0.000	0.000		0.000	0.000		0.000	0.000		0.103	0.005
Thermal	0.310	0.049		0.310	0.049		0.000	0.000		0.600	0.095		0.248	0.039
Parts	0.010	0.010		0.010	0.010		0.030	0.030		0.011	0.011		0.012	0.012
Chemicals	0.050	0.050		0.080	0.080		0.070	0.070		0.010	0.010		0.010	0.010
Labour	0.080	0.080		0.080	0.080		0.100	0.100		0.020	0.020		0.042	0.042
Membranes	0.000	0.000		0.000	0.000		0.030	0.030		0.000	0.000		0.000	0.000
Electrical	0.600	0.600		0.420	0.420		0.720	0.720		0.185	0.185		0.180	0.180
Capital cost	0.420	0.420		0.350	0.350		0.290	0.290		0.430	0.430		0.197	0.197

Cost of electricity is taken at US$0.15 /kWh, the exergy ratio for Turbine to MED is 0.9563 to 0.0437,
Increase in water production by MEDAD is 2 folds of the conventional MED.

Figure 16. A comparison of life-cycle unit water cost for various desalination methods

as shown in Figure 16. Exergy factor calculated above is utilized only for thermal and electricity cost calculations. Energy based analysis has good agreement with GWI [56] data. It can be seen that by LCC, unit water production cost is highest for PP+MSF which amounts to US$ 1.201/m^3, whilst the lowest unit cost is the PP+MEDAD method which is only at US$ 0.485/m^3 and this unit cost is even lower than the LCC of reverse osmosis (RO) plants.

6. Summary

Recent developments in adsorption theory, adsorption desalination (AD), and conventional MED desalination cycles have been reviewed in this chapter. We highlight the key role of AD cycles which can be hybridized with the proven cycles such as the MED cycle, exploiting the thermodynamic synergy between the thermally driven cycles that significantly improve the water production yields. Experiments were conducted in a lab-scale pilot MEDAD and confirmed the excellent synergetic effects that boosted the water production up to two- to threefold over the conventional MED. We believe that if the hybrid MEDAD cycles are well optimized and operated, it can achieve high GOR and the projected LCC of water production can be lowered to as low as US$ 0.485/m^3.

7. Abbreviation

MED; Multi-effect desalination

AD; Adsorption desalination

RO; Reverse osmosis

SDWP; Specific daily water production

EDF; Energy distribution function

GOR ; Gain output ratio

SG; Steam generator

PR; Performance ratio

WPR; Water production ratio

TBT; Top brine temperature

PP; Power plant

HP-T; High pressure turbine

LP-T; Low pressure turbine

LBT; Lower brine temperature

LCC; Life cycle costing

PDF; Probability distribution function

Symbols	
P	Pressure [kPa]
P_0	Saturation pressure [kPa]
R	Universal gas constant [kJ/kmol.K]
T	Temperature [K]
t	Surface heterogeneity for Tóth [-]
Greek Symbols	
γ	Dubinin–Astakhow power factor [-]
ε	Adsorption site energy [kJ/kmol, or kJ/kg]
ε_c	Equilibrium adsorption site energy [kJ/kg]
$\varepsilon_{1\,to\,}\varepsilon_3$	Reference energy [kJ/kmol]
θ	Adsorption uptake [kg/kg of adsorbent]

θ	Local adsorption uptake [kg/kg of adsorbent]	
μ	Chemical potential [kJ/kmol]	
$\chi(\varepsilon)$	Energy distribution function [-]	
Subscript		
α	Adsorbed phase	
g	Gaseous phase	

Acknowledgements

Author details

Muhammad Wakil Shahzad[1*], Kyaw Thu[2], Ang Li[2], Azhar Bin Ismail[1] and Kim Choon Ng[2]

*Address all correspondence to: muhammad.shahzad@kaust.edu.sa

1 King Abdullah University of Science & Technology, Water Desalination & Reuse Center (WDRC), Thuwal, Saudi Arabia

2 Department of Mechanical Engineering, National University of Singapore, Singapore

References

[1] Sources of fresh water, UNESCO module-7 (http://amper.ped.muni.cz/~miler/aktivity/unesco/Science%20and%20Technology%20Education/07_Sources+of+fresh+water.pdf)

[2] http://sciencenordic.com/earth-has-lost-quarter-its-water

[3] Earth's water supply (http://gen.uga.edu/documents/water/Earth.pdf)

[4] National oceanic and atmospheric administration, United State department of commerce. (http://oceanservice.noaa.gov/facts/wherewater.html)

[5] The encyclopedia of earth (http://www.eoearth.org/view/article/152861/)

[6] http://www.universetoday.com/65588/what-percent-of-earth-is-water/

[7]   Science education resource center, Carleton College, (http://serc.carleton.edu/eslabs/index.html)

[8]   Hoekstra AY, Mekonnen MM. Global water scarcity: the monthly blue water footprint compared to blue water availability for the world's major river basins, Value of water research report series no. 53, UNESCO-IHE Institute for Water Education.

[9]   Thu K, Chakraborty A, Kim Y-D, Myat A, Saha BB, Ng KC. Numerical simulation and performance investigation of an advanced adsorption desalination cycle. Desalination 2013;308:209–18.

[10] GWI, Desalination Markets 2007, A Global Industry Forecast (CD ROM), Global Water Intelligence, Media Analytics Ltd., Oxford, UK, 2007, www.globalwaterintel.com

[11] Dawoud MA, Al Mulla MM. Environmental impacts of seawater desalination: Arabian Gulf case study. Int J Environ Sustain 2012;1(3),22–37.

[12] Dawoud MA. The role of desalination in augmentation of water supply in GCC countries, Desalination 2005;186:187–98.

[13] Abdulrazzak MJ. Water supplies versus demand in countries of Arabian Peninsula. J Water Res PL ASCE 1995;121(3):227–34.

[14] Fath H, Sadik A, Mezher T. Present and future trend in the production and energy consumption of desalinated water in GCC countries. Int J Thermal Environ Eng 2013;5(2):155–65.

[15] Nezhad H. A report on world energy scenarios to 2050: issues and options, Decision Sciences Metropolitan State University Minneapolis, MN, Sep-2009.

[16] Al-Zubari WK. The Water-Energy Nexus in the GCC Countries Evolution and Related Policies, Sixth "Zayed Seminar" on Green Economy: Success Stories from the GCC, 8–9 May 2013, UN virtual water learning center, the Arabian regional center, Arabian Gulf University, Bahrain.

[17] Clean Water for a Healthy World, Secretariat of the Convention on Biological Diversity. 2009. Drinking Water, Biodiversity and Poverty Reduction: A Good Practice Guide, World water day March 22, 2010.

[18] Caron DA, Garneau ME, Seubert E, Howard MDA, Darjany L, Schnetzer A, Cetinic I, Filteau G, Lauri P, Jones B, Trussell S. Harmful algae and their potential impacts on desalination operations off southern California. Water Res 2010;44:385–416.

[19] Huttner KR. Overview of existing water and energy policies in the MENA region and potential policy approaches to overcome the existing barriers to desalination using renewable energies. Desalin Water Treat 2013;51:87–94.

[20] Ghaffour N, Missimer TM, Amy GL. Combined desalination, water reuse, and aquifer storage and recovery to meet water supply demands in the GCC/MENA region. Desalin Water Treat 2013;51:38–43.

[21] Langmuir I. The adsorption of gases on plane surfaces of glass, mica and platinum, J Am Chem Soc 1918;40:1361–403.

[22] Ward C, Findlay R, Rizk M. Statistical rate theory of interfacial transport. I. Theoretical development. J Chem Phys 1982;76:5599–605.

[23] Elliott JAW, Ward CA. Statistical rate theory description of beam-dosing adsorption kinetics, J Chem Phys 1997;106:5667–76.

[24] Elliott JAW, Ward CA. Statistical rate theory and the material properties controlling adsorption kinetics, on well defined surfaces. Stud Surf Sci Catal 1997;104:285–333.

[25] Elliott JAW, Ward CA. Temperature programmed desorption: a statistical rate theory approach, J Chem Phys 1997;106:5677–84.

[26] Rudzinski W, Borowiecki T, Dominko A, Panczyk T. A new quantitative interpretation of temperature-programmed desorption spectra from heterogeneous solid surfaces, based on statistical rate theory of interfacial transport: the effects of simultaneous readsorption. Langmuir 1999;15:6386–394.

[27] Rudzinski W, Lee S-L, Panczyk T, Yan C-CS. A fractal approach to adsorption on heterogeneous solids surfaces. 2. Thermodynamic analysis of experimental adsorption data. J Phys ChemB 2001;105:10857–66.

[28] Rudzinski W, Lee S-L, Yan C-CS, Panczyk T. A fractal approach to adsorption on heterogeneous solid surfaces. 1. The relationship between geometric and energetic surface heterogeneities. J Phys Chem B 2001;105:10847–56.

[29] Li A. Experimental and theoretical studies on the heat transfer enhancement of adsorbent coated heat exchangers, Doctor of Philosophy, Department of Mechanical Engineering, National University of Singapore, 2014.

[30] Wang X, Chakarborty A, Ng KC, Saha BB. How heat and mass recovery strategies impact the performance of adsorption desalination plant: theory and experiments. Heat Transfer Eng 2007;28:147–53.

[31] Saha BB, Choon NK, Chakarborty A, Thu K. Desalination System and Method, in: W.P. WO2011010205A1 (ed.), 2011.

[32] Thu K. Adsorption desalination: theory & experiments, in: Doctoral Thesis, National University of Singapore, 2010.

[33] Saha BB, Alam KCA, Akisawa A, Kashiwagi T, Ng KC, Chua HT. Two-stage non-regenerative silica gel-water adsorption refrigeration cycle, ASME Advanced Energy Systems Division (Publication) AES 2000;40:65–9.

[34] Ng KC. Recent developments in heat-driven silica gel-water adsorption chillers. Heat Transfer Eng 2003;24:1–3.

[35] Ng KC, Wang XL, Chakraborty A. in: Apparatus and Method for Desalination, 2006.

[36] Ng KC, Saha BB, Chakraborty A, Koyama S. Adsorption desalination quenches global thirst. Heat Transfer Eng 2008;29:845–8.

[37] Wu JW, Hu EJ, Biggs MJ. Thermodynamic cycles of adsorption desalination system. Appli Energy 2012;90:316–22.

[38] Wu JW, Biggs MJ, Pendleton P, Badalyan A, Hu EJ. Experimental implementation and validation of thermodynamic cycles of adsorption-based desalination. Appl Energy 2012;98:190–7.

[39] Boelman EC, Saha BB, Kashiwagi T. Experimental investigation of a silica gel-water adsorption refrigeration cycle – the influence of operating conditions on cooling output and COP. 1995;101:358–66.

[40] Khan MZI, Alam KCA, Saha BB, Akisawa A, Kashiwagi T. Study on a re-heat two-stage adsorption chiller – the influence of thermal capacitance ratio, overall thermal conductance ratio and adsorbent mass on system performance. Appl Thermal Eng 2007;27:1677–85.

[41] Khan MZI, Alam KCA, Saha BB, Akisawa A, Kashiwagi T. Performance evaluation of multi-stage, multi-bed adsorption chiller employing re-heat scheme. Renewable Energy 2008;33:88–98.

[42] Ng KC, Thu K, Saha BB, Chakraborty A. Study on a waste heat-driven adsorption cooling cum desalination cycle. Int J Refrigeration 2012;35:685–93.

[43] Thu K, Ng KC, Saha BB, Chakraborty A, Koyama S. Operational strategy of adsorption desalination systems. Int J Heat Mass Transfer 2009;52:1811–6.

[44] EI-Sharkawy I, Thu K, Ng K, Saha BB, Chakraborty A, Koyama S. Performance improvement of adsorption desalination plant: experimental investigation. Int Rev Mech Eng 2007;1:25–31.

[45] Ng KC, Wang X, Lim YS, Saha BB, Chakarborty A, Koyama S, Akisawa A, Kashiwagi T. Experimental study on performance improvement of a four-bed adsorption chiller by using heat and mass recovery. Int J Heat Mass Transfer 2006;49:3343–8.

[46] Wang X, Ng KC. Experimental investigation of an adsorption desalination plant using low-temperature waste heat. Appl Thermal Eng 2005;25:2780–9.

[47] Ng KC, Wang XL, Gao LZ, Chakraborty A, Saha BB, Koyama S. Apparatus and method for desalination, SG Patent application number 200503029-1 (2005) and WO Patent no. 121414A1 (2006).

[48] Ng KC, Thu K, Amy G, Chunggaze M, Al-Ghasham TY. An Advanced ADMED Cycle For Low-Temperature Driven Desalination, US Provisional Application No. 61/450,165.

[49] Ng KC, Thu K, Amy G, Chunggaze M, Ghasham TYA. A Regenerative Adsorption Distillation System, in: WO Patent WO2012121675A1, 2012.

[50] Shahzad MW, Ng KC, Thu K, Saha BB, Chun WG. Multi effect desalination and adsorption desalination (MEDAD): a hybrid desalination method. Appl Thermal Eng 2014;72:289–97.

[51] Thu K, Kim Y-D, Amy G, Chun WG, Ng KC. A synergetic hybridization of adsorption cycle with the multi-effect distillation (MED). Appl Thermal Eng 2014;62:245–55.

[52] Ng KC, Thu K, Oh SJ, Ang L, Shahzad MW, Ismail AB. Recent developments in thermally-driven seawater desalination: Energy efficiency improvement by hybridization of the MED and AD cycles. Desalination 2015;356:255–70.

[53] Ng KC, Thu K, Shahzad MW, Chun W. Progress of adsorption cycle and its hybrids with conventional multi-effect desalination processes. IDA J Desalin Water Reuse, DOI 10.1179/2051645214Y.0000000020.

[54] Shahzad MW, Myat A, Chun WG, Ng KC. Bubble-assisted film evaporation correlation for saline water at sub-atmospheric pressures in horizontal-tube evaporator. Appl Thermal Eng 2013;50:670–6.

[55] Lattemann S, Kennedy MD, Schippers JC, Amy G. Chapter 2; Global Desalination Situation.

[56] http://www.globalwaterintel.com/archive/13/10/general/technology-choice-still-open-yanbu-3.html